Article

A wireless patch for the monitoring of C-reactive protein in sweat

Check for updates

Jiaobing Tu[1], Jihong Min [1], Yu Song [1], Changhao Xu [1], Jiahong Li[1], Jeff Moore [2], Justin Hanson [3], Erin Hu [3], Tanyalak Parimon[4], Ting-Yu Wang[5], Elham Davoodi[1], Tsui-Fen Chou[5], Peter Chen[4], Jeffrey J. Hsu[3], Harry B. Rossiter [2] & Wei Gao [1] ✉

The quantification of protein biomarkers in blood at picomolar-level sensitivity requires labour-intensive incubation and washing steps. Sensing proteins in sweat, which would allow for point-of-care monitoring, is hindered by the typically large interpersonal and intrapersonal variations in its composition. Here we report the design and performance of a wearable and wireless patch for the real-time electrochemical detection of the inflammatory biomarker C-reactive (CRP) protein in sweat. The device integrates iontophoretic sweat extraction, microfluidic channels for sweat sampling and for reagent routing and replacement, and a graphene-based sensor array for quantifying CRP (via an electrode functionalized with anti-CRP capture antibodies-conjugated gold nanoparticles), ionic strength, pH and temperature for the real-time calibration of the CRP sensor. In patients with chronic obstructive pulmonary disease, with active or past infections or who had heart failure, the elevated concentrations of CRP measured via the patch correlated well with the protein's levels in serum. Wearable biosensors for the real-time sensitive analysis of inflammatory proteins in sweat may facilitate the management of chronic diseases.

Inflammatory processes and immune responses are associated with a broad spectrum of physical and mental disorders that contribute substantially to modern morbidity and mortality globally. The top-three leading causes of death worldwide, namely, ischaemic heart disease, stroke and chronic obstructive pulmonary disease (COPD), are each characterized by chronic inflammation[1–3]. Although the acute inflammatory response is a critical survival mechanism, chronic inflammation contributes to long-term silent progression of disease through irreversible tissue damage[4–6]. In addition, delayed diagnosis and treatment of chronic diseases impose heavy financial burdens on patients and the healthcare systems[2,4]. A readily available means of monitoring inflammatory biomarkers at home could improve patient outcomes and lower cost factors by monitoring disease progression and prompting the initiation of early treatment and intervention[7].

Although there is no canonical standard biomarker for the measurement and prediction of systemic chronic inflammation[6], C-reactive protein (CRP), an acute-phase protein synthesized by hepatocytes in response to a wide range of both acute and chronic stimuli, has a close association with chronic inflammation and with mortality risk in several disease states (Fig. 1a)[8–12]. The stable nature of CRP in plasma, the absence of circadian variation and its insensitivity to common medications, such as corticosteroids, render it extremely attractive to clinicians as a handy means to assess a patient's physiological inflammatory state[13]. There is also a growing interest in

[1]Andrew and Peggy Cherng Department of Medical Engineering, Division of Engineering and Applied Science, California Institute of Technology, Pasadena, CA, USA. [2]Division of Respiratory and Critical Care Physiology and Medicine, The Lundquist Institute for Biomedical Innovation at Harbor-UCLA Medical Center, Torrance, CA, USA. [3]Division of Cardiology, University of California Los Angeles, Los Angeles, CA, USA. [4]Department of Medicine, Women's Guild Lung Institute, Cedars-Sinai Medical Center, Los Angeles, CA, USA. [5]Proteome Exploration Laboratory, Beckman Institute, California Institute of Technology, Pasadena, CA, USA. ✉e-mail: weigao@caltech.edu
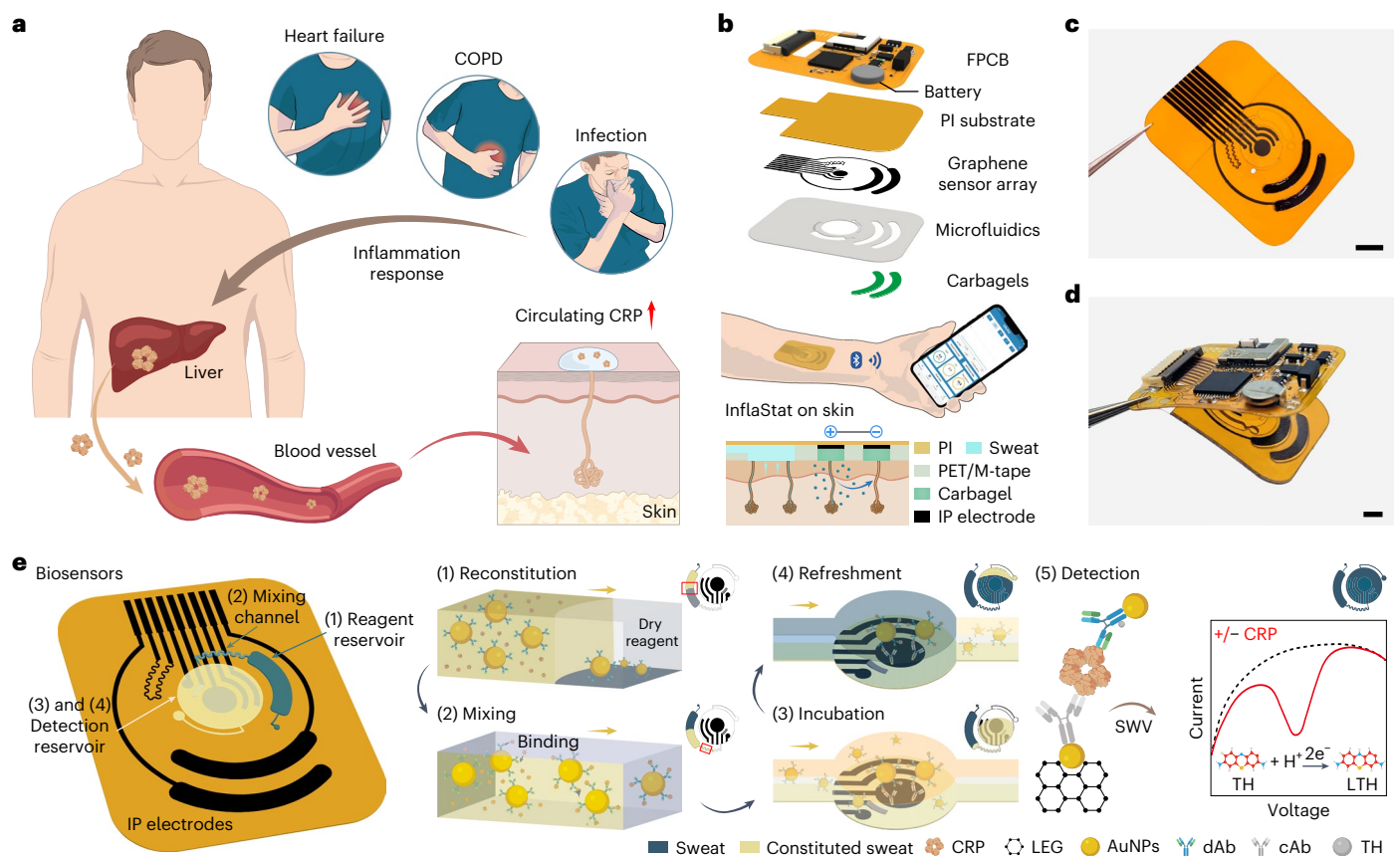
Fig. 1 | Wearable electrochemical biosensor for the automatic, non-invasive and wireless monitoring of inflammation. a, Circulating CRP, released from inflammatory responses, is closely related to various chronic and acute health conditions and could be secreted via the sweat gland. **b**, Schematic of the skin-interfaced wearable biosensor that contains an iontophoretic module for localized sweat extraction on-demand, a microfluidic module for automated sweat sampling and reagent routing and a flexible LEG sensor array for multiplexed sensing of sweat CRP, pH, temperature and ionic strength. **c**,**d**, Optical images of a disposable microfluidic graphene sensor patch (**c**) and a vertical stack assembly of the fully integrated wireless wearable system (**d**). Scale bars, 0.5 cm. **e**, The mechanism of in situ microfluidic sweat CRP analysis that involves fully automatic sweat sampling, reagent routing and detection. Yellow arrows represent the flow direction of reconstituted sweat-reagent mixture. Red boxes highlight the locations in the microfluidic module which the cross-sectional schematics (1) and (2) represent. Carbagel, carbachol hydrogel; IP, iontophoresis; LTH, leuco-thionine; M-tape, medical tape.

exploring the effectiveness of serial CRP measurements for therapeutic decision-making[14,15].

At present, circulating CRP levels are clinically assessed in specific laboratories that rely on invasive blood draws from patients (Supplementary Table 1). Commercial point-of-care CRP monitors are still bulky in size and cannot reach picomolar-level sensitivity to assess CRP levels in non-invasively accessible alternative biofluids, such as sweat and saliva (Supplementary Table 2). A faster, sensitive, non-invasive and user-friendly approach, accessible to clinicians, patients and caregivers, could unleash the full potential of inflammatory biomarker monitoring for clinical management beyond hospital settings.

Recent advances in flexible electronics and digital health have transformed conventional laboratory tests into remote wearable molecular sensing that enables real-time monitoring of physiological biomarkers[16-24]. Sweat contains abundant biochemical molecules, ranging from electrolytes and metabolites to large proteins[25,26], and, importantly, sweat is readily accessible by non-invasive techniques (Fig. 1a). However, currently reported wearable biosensors are largely restricted to the detection of a limited selection of biomarkers, such as electrolytes and metabolites, at micromolar or greater concentrations via ion-selective and enzymatic sensors or via direct redox reactions[16,20,27-40]. The majority of clinically relevant protein biomarkers including CRP are present at nanomolar to picomolar levels in blood, whereas the anticipated levels of proteins in sweat are expected to be

much lower than those in blood[26]. Despite recent efforts in the development of wearable bioaffinity biosensors for trace-level biomarkers, such as cortisol, the accurate and in situ detection of protein biomarkers in sweat remains a major challenge owing to their extremely low concentrations (picomolar levels) and the large interpersonal and intrapersonal variations in sweat composition[41-44]. The detection of protein biomarkers usually requires integrating bioaffinity receptors, such as antibodies and aptamers[43,45]. However, such techniques typically require lengthy target incubation, labour-intensive washing steps and the addition of redox solutions for signal transduction. Thus, there is a strong desire for a wearable biosensing technology that allows automatic in situ monitoring of ultralow levels of circulating proteins at home and in community settings.

Here we report a wireless wearable biosensor, InflaStat, for non-invasive personalized monitoring of inflammatory status (Fig. 1b–e). The InflaStat consists of an autonomous iontophoresis module for on-demand and controlled sweat extraction; a sweat-gland-powered, skin-interfaced microfluidic module that capitalizes on sweat flow to achieve fully automated protein and detector antibody (dAb) capturing, subsequent washing and picomolar-level electrochemical detection on the skin; and a flexible nanoengineered multiplexed sensor array for in situ sweat inflammatory biomarker analysis. The use of gold nanoparticle (AuNP)-decorated, mass-producible laser-engraved graphene (LEG) enables highly sensitive and efficient electrochemical

detection of trace-level sweat CRP in situ on the skin. AuNPs conjugated with electroactive redox molecule thionine (TH) and dAb enable efficient electrochemical signal transduction (signal ON) and further signal amplification. The integrated graphene sensors for measuring pH, temperature and ionic strength enable real-time, personalized CRP data calibration to mitigate the interpersonal sample matrix variation-induced sensing errors, and provide a more comprehensive assessment of the inflammatory status[46,47]. We confirmed the presence of CRP in human sweat from healthy participants, and identified elevated sweat CRP levels in patients with chronic and acute inflammations associated with COPD, heart failure (HF), and active and past infections (such as coronavirus disease 2019 (COVID-19)). A strong correlation between sweat and serum CRP levels was obtained in both healthy and patient populations, indicating the utility of this technology for non-invasive disease classification, monitoring and management.

Results

Design of the wearable microfluidic LEG–AuNPs biosensor

Key components of the wearable sensor are a skin-interfaced, flexible, disposable, multiplexed microfluidic biosensor patch fabricated on a polyimide (PI) substrate via CO_2 laser engraving and a flexible printed circuit board (FPCB) for iontophoretic sweat induction, sensor data acquisition and wireless communication (Fig. 1b and Supplementary Fig. 1). The sensor array consists of an electrodeposited AuNP-decorated LEG working electrode immobilized with anti-CRP capture antibodies (cAbs), a Ag/AgCl reference electrode, an LEG counter electrode for sweat CRP capturing and electrochemical analysis, an LEG-based impedimetric ionic strength sensor, an LEG–polyaniline-based potentiometric sweat pH sensor and a strain-insensitive resistive graphene temperature sensor (Supplementary Fig. 2). Considering that the potential users of this technology include patients who are sedentary and immobile, an iontophoresis module (based on a pair of LEG electrodes) is incorporated for on-demand delivery of cholinergic agonist carbachol from the carbachol hydrogel for autonomous sweat stimulation throughout daily activities without the need for vigorous exercise. A cost-effective and flexible microfluidic module is assembled by stacking laser-cut medical adhesives and polyethylene terephthalate (PET) for efficient sweat sampling (Fig. 1c). The miniaturized FPCB interfaces compactly on top of the microfluidic sensor patch to form the fully integrated wearable system (Fig. 1d). Powered by a small onboard lithium battery, the wearable system is able to wirelessly communicate with a user interface via Bluetooth Low Energy (BLE; Supplementary Fig. 3).

To realize automatic wearable CRP detection in situ, the microfluidic module comprises a reagent reservoir for the storage of the labelled anti-CRP dAb-conjugated AuNPs, a serpentine mixing channel for mixing of dAb with sweat CRP, and a detection reservoir for the capture and quantification of sweat CRP (Fig. 1e and Supplementary Video 1). The redox molecule, TH, is used to label the nanoparticle conjugates to achieve direct electrochemical sensing. As the autonomously induced sweat flows into the microfluidics, the deposited dAb-conjugated AuNPs are reconstituted within the reagent reservoir ((1) in Fig. 1e) and routed along with sweat through a serpentine passive mixer to facilitate the dynamic binding between sweat CRP and dAb ((2) in Fig. 1e). As the mixture enters the detection reservoir, it slowly fills the chamber before exiting via the outlet; the detection reservoir has an optimized size to allow sufficient time for the CRP dAb to bind with the anti-CRP cAb-functionalized LEG–AuNPs working electrode ((3) in Fig. 1e). Subsequently, a fresh sweat stream continues to refresh the microfluidics to achieve passive label removal ((4) in Fig. 1e). Square wave voltammetry (SWV) is used to measure the amount of TH bound to the working electrode surface. As TH molecules are directly conjugated to CRP dAb-immobilized AuNPs, their amount bound is directly correlated to the amount of CRP 'sandwiched' between cAbs at the electrode surface and dAb-immobilized AuNPs and, consequently, the initial concentration of CRP in solution.

Materials and electrochemical characterizations of the LEG–AuNPs immunosensor

The functionalization process for the preparation of the CRP immunosensor is illustrated in Fig. 2a and Supplementary Fig. 4. AuNPs are electrodeposited on the LEG surface followed by subsequent thiol monolayer assembly with mercaptoundecanoic acid (MUA) and mercaptohexanol (MCH). As the formation of the self-assembled monolayer (SAM) relies on specific gold–sulfur bonding, immersion of the sensor patch in alkanethiol solution has negligible influence on other graphene-based electrodes (Supplementary Fig. 5). Pulsed potential-deposited AuNPs evenly distribute throughout the mesoporous graphene structure, possess superior electrocatalysis capability and form a large number of binding sites on the surface of the particles for biomolecule immobilization (Fig. 2b,c and Supplementary Fig. 2b). This substantially improves the sensitivity of the CRP sensor with little non-specific adsorption (Supplementary Fig. 6). The formation of the LEG–AuNPs composite is confirmed through the increased ratio of the intensity of D and G bands in the Raman spectra due to the presence of AuNPs (Fig. 2d)[48]. The individual sensor-modification steps on the LEG electrodes are characterized with X-ray photoelectron spectroscopy (XPS; Fig. 2e and Supplementary Fig. 7). The intensity of Au 4f increases substantially after the deposition of AuNPs, while N 1s increases only after the cAb immobilization step, indicating successful electrode preparation (Fig. 2e). Differential pulse voltammetry (DPV) and electrochemical impedance spectroscopy were used to further characterize the LEG surface electrochemically after each modification step (Fig. 2f and Supplementary Fig. 8). The decrease in peak current height in DPV voltammograms and increased resistance in Nyquist plots after SAM and cAb protein immobilization indicate that SAM and cAb impede the electron transfer at the interface. This is due to the increase in surface coverage by non-conductive species. Moreover, the negatively charged carboxylate functional groups in the SAM result in the repulsion of the negatively charged redox indicator, ferricyanide, and further reduces the electron transfer rate. Subsequent modification of the SAM with N-(3-dimethylaminopropyl)-N'-ethylcarbodiimide (EDC)–N-hydroxysuccinimide (NHS) chemistry replaces the negatively charged carboxylate groups with neutral NHS–ester groups. This is empirically observed as an increase in peak current height. Such electrode fabrication processes show high batch-to-batch reproducibility as the main processes, including laser engraving, electrochemical deposition and solution process, are all mass-producible (Supplementary Fig. 9).

To realize trace-level sweat CRP analysis, PEGylated AuNPs that possess a large surface area-to-volume ratio are functionalized with polystreptavidin R (PS-R) to increase the loading of biotinylated dAbs and subsequently enhance the sensitivity (Supplementary Figs. 10 and 11). One-step direct electrochemical detection is enabled by crosslinking the redox label TH onto the carboxylate residues on the dAb-loaded AuNPs. As the TH-labelled, dAb-loaded AuNPs bind to the mesoporous graphene electrode upon CRP recognition, the TH located on the external sites of the proteins is in close proximity to the graphene surface in each mesopore for electron transfer. Increases in hydrodynamic sizes (Fig. 2g) and the shifts of ultraviolet–visible (UV–vis) absorbance (Supplementary Fig. 12) of the AuNPs conjugate after each modification step, along with the transmission electron microscope image of the dispersed AuNP–dAb conjugates (Fig. 2h), confirm the successful immobilization of the dAbs.

The performance of the CRP sensor was evaluated with SWV in CRP-spiked phosphate-buffered saline (PBS) solutions (Fig. 2i). The increases in peak current height of TH reduction show a linear relationship with increased target concentrations (Fig. 2j). The sensor showed an ultralow limit of detection of 8 pM and good batch-to-batch reproducibility (Supplementary Fig. 13), and the sensing accuracy can be further enhanced by automating the sensor preparation and modification
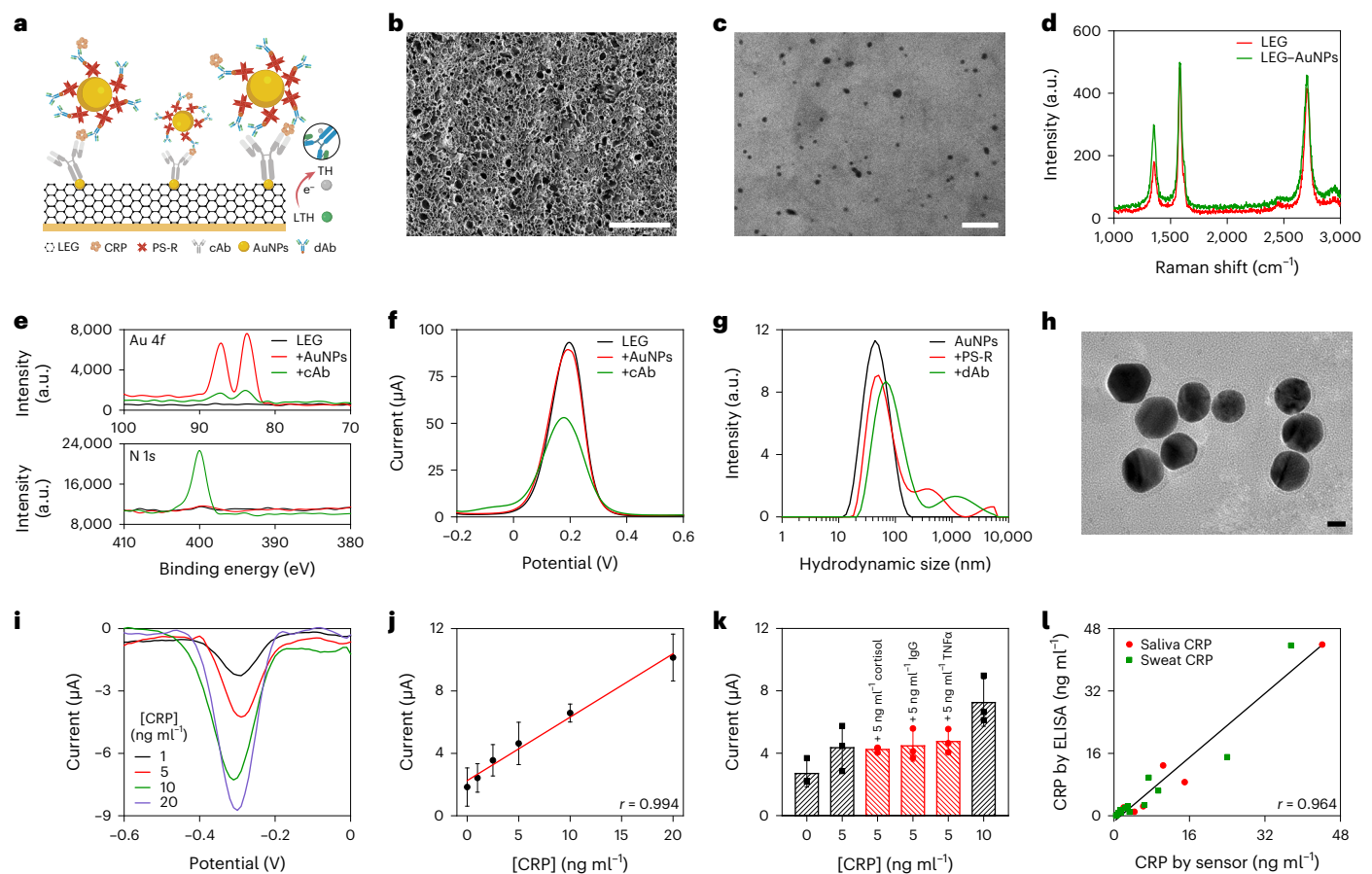
Fig. 2 | Materials and electrochemical characterizations of the LEG–AuNPs CRP sensor. a, Schematic of the one-step electrochemical sandwich CRP immunosensor. **b**, Scanning electron microscope image of the mesoporous LEG electrode. Scale bar, 100 µm. **c**, Transmission electron microscopy image of AuNP-decorated graphene flakes. Scale bar, 50 nm. **d**, Raman spectra of LEG electrode and AuNP-decorated LEG electrode. **e**, X-ray photoelectron spectra of the LEG after the deposition of AuNPs, thiol-based SAM and cAb immobilization. **f**, DPV voltammograms of a sensing electrode in a 0.1 M KCl solution containing 5.0 mM $K_4Fe(CN)_6$–$K_3Fe(CN)_6$ (1:1) after each surface-modification step: bare LEG, deposition of AuNPs, SAM modification, carboxylic acid group activation with EDC–sulfo-NHS and cAb immobilization followed by BSA blocking. **g**, Hydrodynamic sizes of the PEGylated AuNPs after each

conjugation step by dynamic light scattering: PS-R immobilization, biotinylated dAb binding and redox molecule TH conjugation followed by BSA deactivation. **h**, Transmission electron microscopy image of the dispersed dAb-loaded AuNPs with protein corona shells. Scale bar, 10 nm. **i,j**, SWV voltammograms (**i**) and the corresponding calibration plot (**j**) of the CRP sensors in 1× PBS (pH 7.4) with 0–20 ng ml⁻¹ CRP and 1% BSA. Error bars represent the s.d. of the mean from three sensors. **k**, Selectivity of the CRP sensor to potential interferences in sweat. Error bars represent the s.d. of the mean from three sensors. **l**, Validation of the CRP sensor in human sweat samples (n = 13 biological replicates) and saliva samples (n = 6 biological replicates) with ELISA. Pearson correlation coefficient was acquired through linear regression.

process (that is, via automated fluid dispensing or inkjet printing[49]). The LEG–AuNPs CRP immunosensor demonstrates high selectivity over other potential interference proteins and hormones attributed to the sandwich assay format (Fig. 2k and Supplementary Fig. 14). Considering interpersonal variations during the human study, the influence of sweat pH, ionic strength, temperature, and sample volume on the antibody–antigen binding kinetics and redox probe electron transfer rate on CRP sensing accuracy was investigated (Supplementary Fig. 15) and mitigated by introducing suitable calibration mechanisms. The potential variations of the Ag/AgCl pseudo-reference electrode in the presence of varying Cl⁻ concentration in the physiologically relevant range result in a small shift in the peak potential, but its influence on the overall peak current density (and thus CRP quantification) is negligible (Supplementary Fig. 16). The accuracy of the CRP sensor for biofluid analysis was validated by the laboratory gold-standard enzyme-linked immunosorbent assay (ELISA) using human sweat and saliva samples (Fig. 2l). The disposable CRP sensors also maintained stable sensor performance over a 10 day period when stored in PBS in the refrigerator at 4 °C (Supplementary Fig. 17).

Evaluation of sweat CRP for the non-invasive monitoring of systemic inflammation

Despite the high potential of non-invasive CRP monitoring, the presence and levels of CRP in sweat are extremely underexplored in the literature[50]. To affirm the presence of CRP in sweat generated by iontophoresis and by vigorous exercise, we first conducted a proteomic characterization of different types of sweat samples using bottom-up proteomic analysis, as illustrated in Fig. 3a. Using a recombinant CRP protein standard as the reference, we identified CRP in both exercise and iontophoretic sweat sample from participants (Fig. 3b, Supplementary Fig. 18 and Supplementary Table 3). In this regard, we further evaluated the use of our LEG–AuNPs CRP sensors for the assessment of sweat CRP as a universal, cost-effective and non-invasive approach to monitor systemic inflammation in various disease states (Fig. 3c and Supplementary Tables 4–6).

We investigated healthy participants grouped according to smoking status (current, former and never smokers), where CRP levels in both serum and sweat were greater in current smokers compared with former and never smokers (Fig. 3d), consistent with previous reports
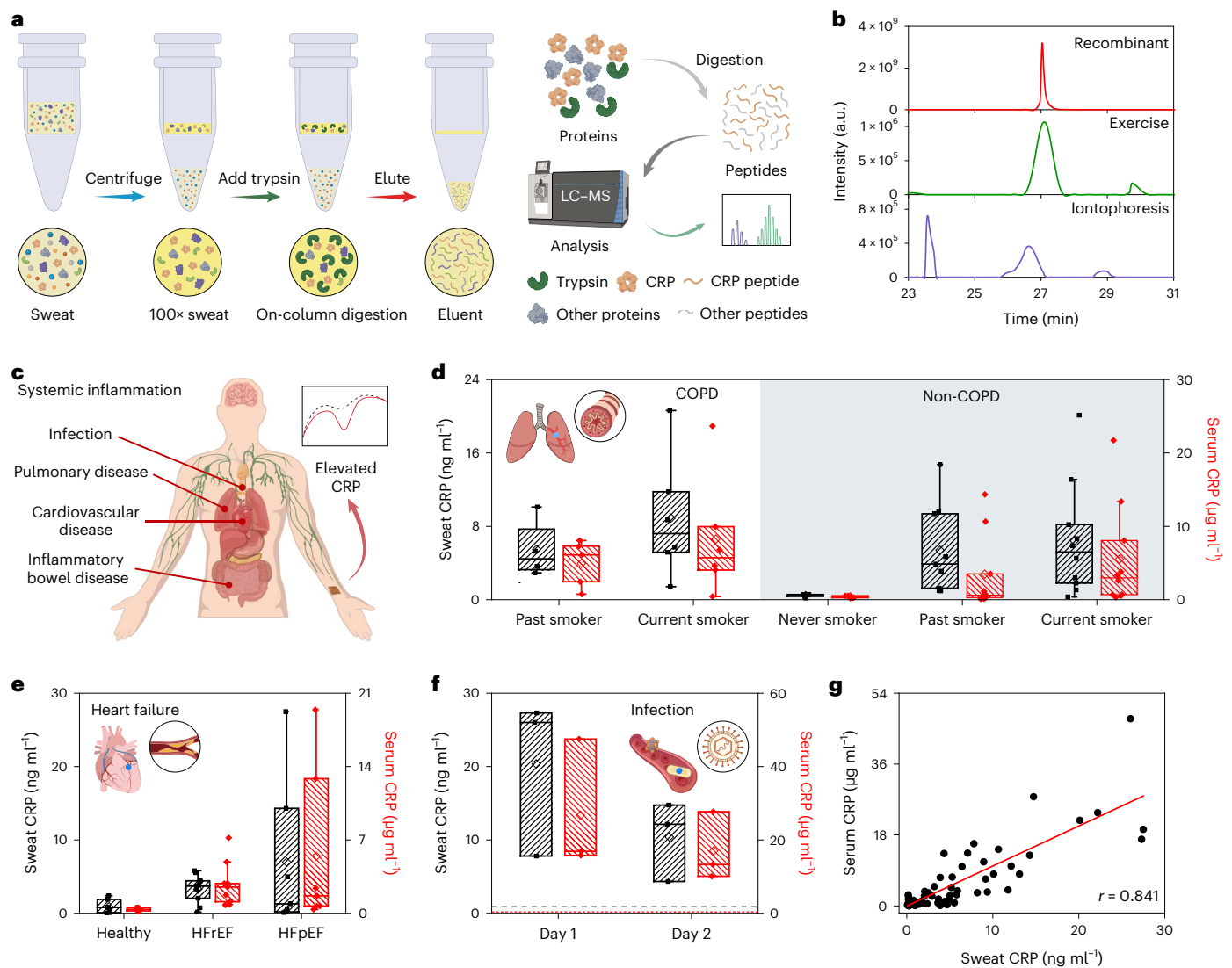
Fig. 3 | Evaluation of sweat CRP for the non-invasive monitoring of systemic inflammation in healthy and patient populations. a, Schematic of proteomic analysis of human sweat using LC–MS/MS. **b**, Chromatograms of the recombinant CRP reference peptide GYSIFSYATKR and iontophoresis-extracted and exercise sweat samples from the participants. **c**, Schematic of the non-invasive inflammation monitoring in various health conditions with the LEG–AuNPs CRP sensor. **d**, Box-and-whisker plot of CRP levels in iontophoresis-extracted sweat and serum samples from the patients with COPD ($n = 10$ biological replicates) and without COPD ($n = 24$ biological replicates). The participants are classified into five subgroups: current smokers with COPD ($n = 6$ biological replicates) or without COPD ($n = 10$ biological replicates), former smokers with COPD ($n = 4$ biological replicates) and without COPD ($n = 9$ biological replicates) and never smokers without COPD ($n = 5$ biological replicates). **e**, Box-and-whisker plot of CRP levels in sweat and serum samples from healthy participants ($n = 7$ biological replicates), patients with HF with reduced ejection fraction (HFrEF; $n = 7$ biological replicates) and patients with HF with preserved ejection fraction (HFpEF; $n = 9$ biological replicates). **f**, Box-and-whisker plot of CRP levels in sweat and serum samples from three patients with active infection on two consequent days ($n = 3$ biological replicates). The dashed lines represent the mean values of the sweat and serum CRP levels for healthy participants. **g**, Correlation of serum and sweat CRP levels. The correlation coefficient r was acquired through Pearson's correlation analysis ($n = 80$, $P < 0.00001$). In panels **d**–**f**, the bottom whisker represents the minimum, the top whisker represents the maximum and the square in the box represents the mean.

on the effect of current smoking on serum CRP[51]. However, among patients with COPD, serum and sweat CRP values were greater in former smokers than current smokers, consistent with irreversible tissue damage and chronic inflammation in patients with COPD even after smoking cessation[52]. Monitoring sweat CRP in patients with COPD may therefore be useful for following disease progression and/or predicting exacerbation in this patient population[53].

Chronic systemic inflammation is also related to increased risks of cardiovascular events[3]. In a preliminary study with patients with HF, our sensor results show that serum and sweat CRP values were substantially elevated in patients with HF with preserved ejection fraction but not in patients with HF with reduced ejection fraction (Fig. 3e),

consistent with past studies[54–57]. The investigation of the dynamics of sweat CRP using our technology could have high value in predicting HF with preserved ejection fraction disease progression and clinical outcomes[55].

In addition to chronic infections in COPD and HF, it is well known that acute infections (such as COVID-19) could lead to severe inflammatory responses[14]. In a pilot study, we evaluated our sensor on hospitalized patients with active infections for two consecutive days (Fig. 3f). A substantial increase (over tenfold on average) in both serum and sweat CRP was identified in patients with active infection compared with healthy participants, indicating the presence of highly elevated sweat CRP in acute inflammation.

By analysing the samples from healthy participants and patient populations with various inflammatory conditions using our sensor, a high correlation coefficient (r) of 0.844 (n = 80) between sweat and serum CRP concentrations was obtained (Fig. 3g). Such a correlation appears to be higher than that obtained from saliva and urine samples (Supplementary Fig. 19), suggesting the great potential of using sweat CRP for the non-invasive monitoring of systemic inflammation towards the management of a variety of chronic and acute health conditions.

Characterization of the multiplexed microfluidic patch for automatic immunosensing

To realize accurate and automatic immunosensing in situ, the flexible sensor patch was designed to have a laser-engraved microfluidic module (consisting of a reagent reservoir, a mixing channel and a detection reservoir) and a multiplexed LEG sensor array (consisting of a CRP immunosensor, an ionic strength sensor and a pH sensor) (Fig. 4a). As the microfluidic module passively routes sweat on the skin, the impedimetric ionic strength sensor automatically captures the state of the detection reservoir (reagent flow and refreshment); the measured admittance signals show a log-linear response with the electrolyte concentrations (Fig. 4b,c). As large interpersonal variations in electrolyte and pH levels were observed in both exercise and chemically induced sweat samples (Supplementary Fig. 20), high-level buffering salts were deposited with the dAbs in the reagent reservoir to mitigate potential binding environment changes caused by sweat composition variations (Supplementary Fig. 21). As such, this introduces an electrolyte gradient between the detection reagent of reconstituted sweat (mixture) and the fresh sweat that subsequently enters the detection reservoir. According to the numerical simulation, the routing of sweat and detection reagents can be summarized into four steps: (1) reconstitution, (2) incubation, (3) refreshment and (4) detection (Fig. 4d,e and Supplementary Note 1). Based on the microfluidic flow test using artificial sweat (0.2× PBS) under a mean physiological sweat rate (1.5 μl min^{-1}), the admittance signal is initially close to zero when no fluid enters the chamber during the reconstitution stage; as reconstituted, high-salt-loaded detection reagents flow into the detection chamber, admittance reaches its peak value and gradually decreases as high-salt-loaded reagents are flushed out of the detection chamber by newly secreted sweat (Fig. 4f). As electrolyte content in iontophoresis sweat remains relatively stable for the same individual[28], the admittance response plateaus after all reagents have been refreshed by natural sweat, indicating the working electrode is ready for electrochemical CRP detection. Further experimental flow testing using fluorescent proteins (fluorescein isothiocyanate (FITC)−albumin as CRP surrogate and peridinin chlorophyll protein as detection reagent) shows a similar trend in incubation and refreshment process as the simulation and electrolyte flow test (Fig. 4g and Supplementary Video 2). Based on sweat rate information collected from 24 current and former smokers with and without COPD (Supplementary Fig. 22), flow tests with flow rates varying from 0.5 μl min^{-1} to 3.5 μl min^{-1} show similar admittance patterns with plateaus after various refreshing processes (Fig. 4h). The gradient of admittance at different flow rates converges to zero as pre-loaded salts and dye are refreshed from the detection reservoir. The mean sweat volume routed during this process before sensor readings were taken was estimated to be 21 μl based on flow rate and admittance measurements (Fig. 4h).

The performance of CRP sensors based on this automated electrolyte monitoring mechanism was evaluated in multiple microfluidic flow tests. SWV electrochemical measurements were initiated during the admittance plateaus (Fig. 4i). An increased concentration (from 1 ng ml^{-1} to 5 ng ml^{-1}) led to an increased SWV peak current height while no substantial difference in CRP sensor response was observed for the same concentration under physiologically relevant flow rates (1 μl min^{-1}, 1.5 μl min^{-1}, 2.5 μl min^{-1} and 3.5 μl min^{-1}) (Fig. 4i,j and Supplementary Fig. 23). Although a higher flow rate could also result in

a faster refreshment of the detection chamber and a thus shorter incubation time for the detection antibody and CRP, the increment in CRP signals under varying incubation times corresponding to the physiologically relevant sweat rates (between 5 min and 20 min) is relatively small (Supplementary Fig. 15). Although the binding condition is pre-adjusted with deposited salts, the flow test with different initial electrolyte concentrations (0.1× and 0.2× PBS were chosen as artificial sweat to simulate interpersonal variations in sweat electrolyte concentrations) shows slightly decreased SWV signals at the lower electrolyte concentration due to the influence of electrolyte levels on the rate of TH reduction (Fig. 4k,l). Similar to in vitro selectivity results, no major interferences on the CRP detection signal were observed in the flow test (Supplementary Fig. 24). Moreover, flow tests using artificial sweat with different pH levels led to varied SWV signals (Supplementary Fig. 25). These results indicate that sweat rate calibration is not necessary while additional in situ signal calibrations with sweat pH and electrolyte levels are needed to mitigate the interpersonal variations on CRP detection accuracy. Compared to previously reported passive wearable microfluidic sensors which rely on vigorous exercise to induce sweat and cannot reach sensitivities below millimolar levels (Supplementary Table 7), our technology offers an attractive, fully automated microfluidic sweat induction, collection and high-accuracy quantitative analysis solution, ideally suitable for at-home monitoring of clinically relevant trace-level biomarkers.

System integration and on-body evaluation of the wearable biosensor

The fully integrated, wearable inflammation monitoring system, InflaStat, is designed based on a vertical stack assembly of a flexible microfluidic sensor patch and FPCB, and can be worn comfortably by the participants (Fig. 5a). As illustrated in the electronic circuit block diagram and schematic in Fig. 5b and Supplementary Fig. 26, the FPCB is able to perform current-controlled iontophoresis, multiplexed electrochemical measurements (including voltammetry, impedimetry and potentiometry), signal processing and wireless communication. The integrated system could also accurately obtain the dynamic responses of the integrated LEG-based pH, ionic strength and skin temperature sensors for real-time CRP sensor calibration (Fig. 5c−f and Supplementary Fig. 27). The InflaStat is designed to have good mechanical flexibility and stability towards practical usage during various physical activities. Each individual sensor shows relatively small variations under a moderate radius of bending curvature (5 cm; Supplementary Fig. 28). More strain-insensitive sensor designs can be included when necessary[58]. During on-body operation, the InflaStat can adhere conformally to the skin through medical adhesive with in situ CRP sensing performed in the microfluidics without direct sensor-skin contact.

Clinical on-body evaluation of the wearable system was performed on healthy participants (involving both never smokers and current smokers), patients with COPD and participants who had recovered from COVID-19 (Fig. 5g−l and Supplementary Figs. 29−31). During the on-body trials, the wearable system laminates conformally on the participant's arm, chemically induces and analyses sweat (Supplementary Video 3 and Supplementary Fig. 32) and acquires inflammatory biomarker information non-invasively and wirelessly (Fig. 5g). The obtained sensor data can be displayed on a custom-developed mobile app in real-time (Fig. 5h). In situ pH, temperature and CRP sensor readings are acquired after the ionic strength sensor indicate full refreshment of the detection reservoir (Fig. 5h−l). It should be noted that the TH reduction peak for the CRP sensor appears at a slightly shifted potential given the variations in sweat pH (Supplementary Fig. 33). The CRP concentration was converted in the mobile app based on the obtained SWV voltammogram and the corresponding real-time-obtained ionic strength, pH and temperature values (Supplementary Fig. 34 and Supplementary Note 2). As expected, an elevated CRP level was observed from the current smokers compared with the
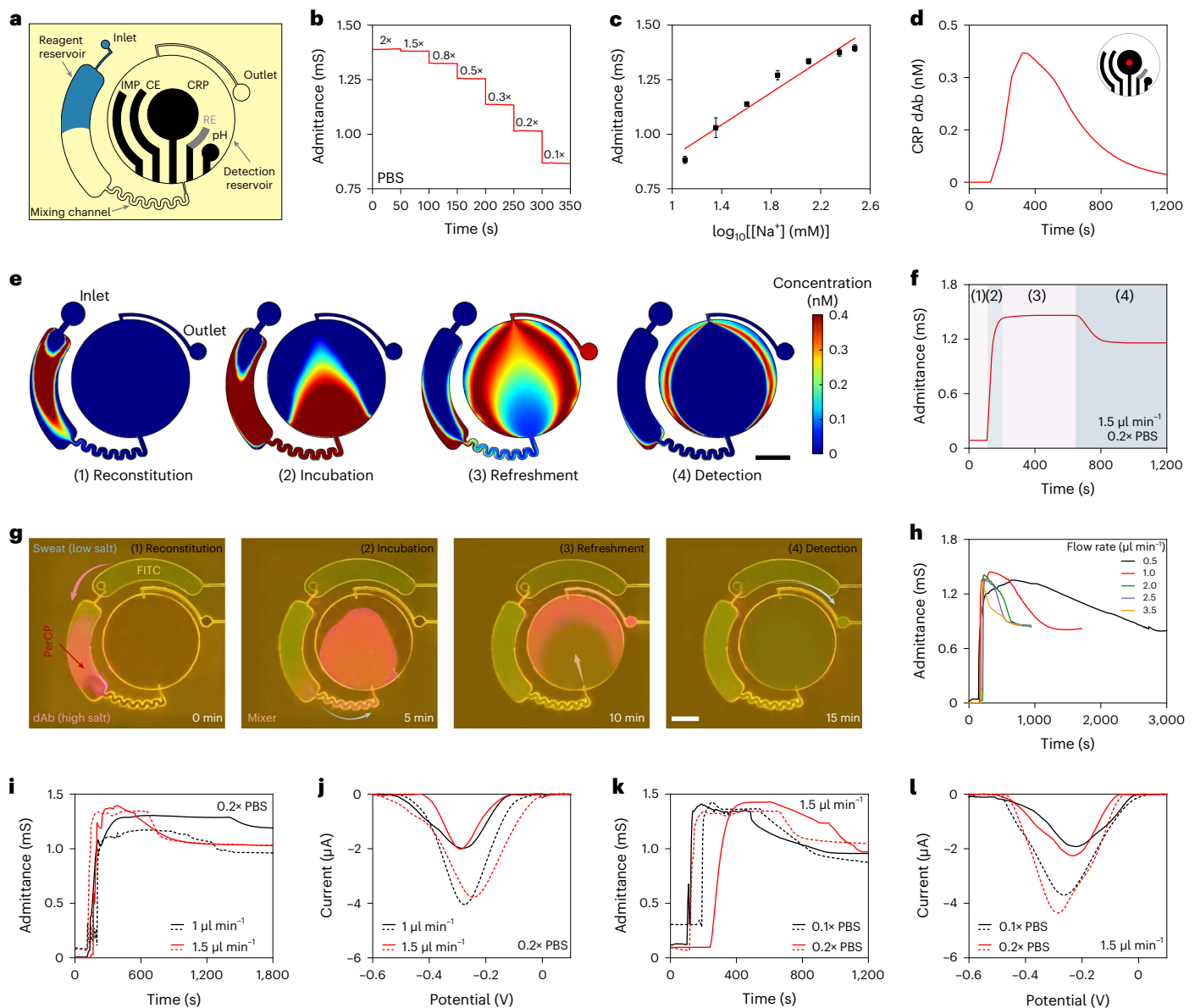
Fig. 4 | Multiplexed microfluidic patch for automatic immunosensing. a, Illustration of the multiplexed sensor array for automatic immunosensing. CE, counter electrode; IMP, impedance electrodes; RE, reference electrode. **b,c,** Admittance responses (**b**) and the corresponding calibration plot (**c**) of the impedimetric ionic strength sensor in NaCl solutions. Error bars represent the s.d. of the mean from three sensors. **d,** Simulated CRP dAb concentration changes on the working electrode over time. The red dot in the inset image indicates the location of the concentration change plot. **e,** Simulated CRP dAb concentration colour maps showing phases of automatic sweat sampling and reagents routing towards in situ CRP detection: (1) reconstitution, (2) incubation, (3) refreshment and (4) detection. Scale bar, 200 μm. **f,g,** Admittance changes of the LEG ionic strength sensor (**f**) and optical images (**g**) during the four stages

(1–4) of the automatic CRP sensing process in a laboratory flow test using artificial sweat (0.2× PBS) at a flow rate of 1.5 μl min⁻¹. Yellow FITC–albumin fluorescent label was used to imitate the flow of sweat CRP and red PerCP was used in place of dAb-loaded AuNPs. Scale bar, 200 μm. **h,** Admittance responses of the ionic strength sensor in artificial sweat (0.2× PBS) at different flow rates from 0.5 μl min⁻¹ to 3.5 μl min⁻¹. **i–l,** Influence of the flow rates (**i,j**) and ionic strengths (**k,l**) on microfluidic automatic CRP sensing. The solid and dashed lines represent tests performed in 1 ng ml⁻¹ and 5 ng ml⁻¹ CRP, respectively. **i** and **j** are impedance signals (**i**) and SWV signals (**j**) obtained from flow tests conducted in 5-fold diluted phosphate buffered saline (0.2× PBS). **k** and **l** are impedance signals (**k**) and SWV signals (**l**) obtained from flow tests conducted at a flow rate of 1.5 μl min⁻¹.

never smokers in healthy participants. The CRP levels in the patients with COPD and participants post-COVID-19 were substantially greater than those of healthy participants who were not smokers, suggesting the promise of using the InflaStat in practical, non-invasive systemic inflammation monitoring and disease management applications. In vitro analysis of sweat and serum from participants recovered from COVID-19 corroborate the on-body observation that individuals who experienced moderate symptoms during COVID-19 may still present a low-grade inflammation post-COVID-19 episode, as indicated by the

slightly elevated CRP levels (Supplementary Fig. 35 and Supplementary Table 8). It should be noted that, similarly to serum, sweat CRP levels remained stable during the test period (Supplementary Fig. 36) and no substantial variations were observed for chemically induced sweat samples at different body locations (Supplementary Fig. 37).

Discussion

We developed a fully integrated, wearable biosensor patch for the real-time, non-invasive monitoring of CRP through automatic in situ
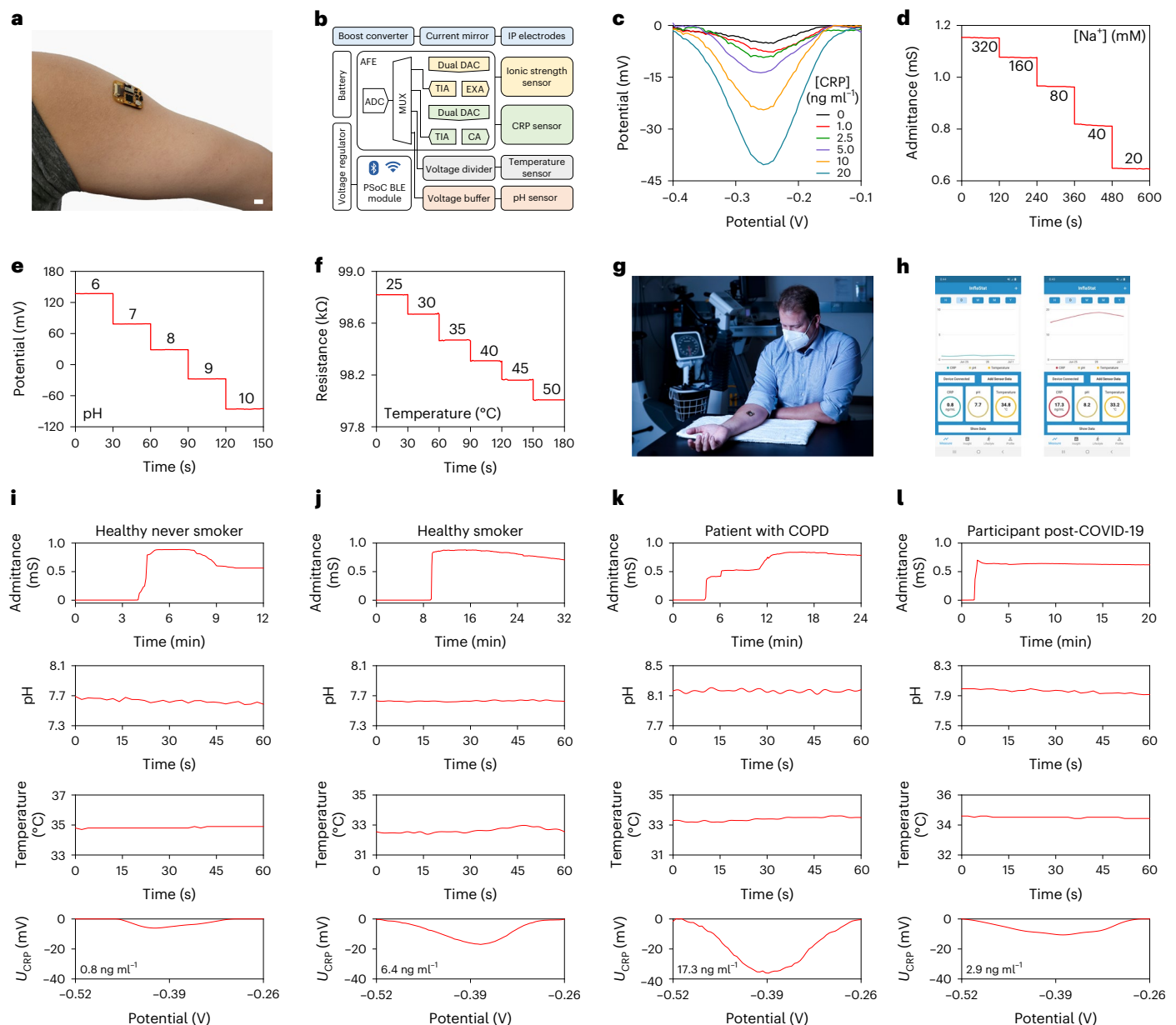
Fig. 5 | On-body evaluation of the multiplexed wearable patch towards non-invasive automatic inflammation monitoring. a, Image of a fully integrated wearable sensor on the arm of a participant. Scale bar, 1 cm. **b**, Block diagram of the electronic system of the InflaStat. ADC, analogue-to-digital converter; AFE, analog front end; CA, control amplifier; DAC, digital-to-analogue converter; EXA, excitation amplifier; MUX, multiplexer; TIA, trans-impedance amplifier. **c–f**, Calibration plots obtained using the wearable system from the CRP (**c**), ionic strength (**d**), pH (**e**) and temperature (**f**) sensors. Error bars represent the s.d. of the mean from three sensors. **g**, Photograph of a participant wearing the sensor patch during a clinical study. **h**, Custom mobile application for real-time data acquisition and display towards inflammation tracking. **i–l**, On-body multiplexed physicochemical analysis and CRP analysis with real-time sensor calibrations using the wearable sensor from a healthy never smoker (**i**), a healthy smoker (**j**), a patient with COPD (**k**) and a participant who previously had COVID-19 (**l**). U_{CRP}, potential of CRP sensor.

microfluidic analysis. The wearable sensor performs autonomous sweat extraction, collection, biomarker analysis and wireless data transmission on-demand across daily human activities in individuals who are sedentary. In contrast with previous wearable technologies for the monitoring of biomarkers and with our previously reported LEG-based sensors, which typically detect metabolites at micromolar (or higher) levels[27,59], this technology realizes the highly sensitive detection of ultralow levels of inflammatory proteins in situ with a six-orders-of-magnitude (picomolar level) improvement in sensitivity through a holistic combination of (1) a nanoengineered immunosensor highly sensitive and selective for CRP analysis; (2) a microfluidic

module for automatic sweat extraction, sampling reagent routing and refreshing; and (3) a multiplexed graphene sensor array for real-time data acquisition and sensor calibration. The operation principle can be readily adapted to survey a broad array of inflammatory biomarkers (such as cytokines).

We assessed the elevation of sweat CRP in healthy participants and in patients with various health conditions (COPD, HF, and active and past infections) for the monitoring of chronic and acute systemic inflammation, and have found a strong correlation between CRP levels in sweat and serum. In practice, the spot checking of CRP every several hours is sufficient to monitor active infections and immune responses. The

disposable point-of-care CRP sensor patch design with a reusable wearable electronic system serves the purpose of immediate, non-invasive, on-the-skin assessment of circulating CRP at any given time. When necessary, dynamic and automatic wearable CRP sensing could be realized by incorporating capillary bursting valves[60] and CRP sensor arrays into a single disposable sensor patch. It is also worth noting that, although the clinical use cases that we have shown in this work do not conform to current clinical practices, the reason behind this disparity is the lack of such specific, immediate and non-invasive inflammation-assessment tools, rather than the lack of needs. The current turnaround time (1 day) of the clinical high-sensitivity CRP test (hsCRP) does not meet this need for frequent assessments. In addition to hospitalized cases, which require the close monitoring of inflammatory state, many chronic diseases, such as COPD and inflammatory bowel disease, could benefit from the at-home, daily or frequent, fully automatic and non-invasive assessment of CRP for disease management.

Outlook

Owing to the accessibility of sweat as a biofluid, the wearable technology here reported enables the acquisition of quantitative, personalized inflammatory information, and may address the unmet needs of patients and caregivers in the context of chronic inflammatory diseases, especially as society progresses towards decentralized medicine. The technology currently enables the interrogation of the dynamicity of CRP, providing clinical insights. Further investigation of the metabolic timeline of CRP in sweat in response to inflammatory stimuli and therapy initiation may provide further insights into the utility of the biomarker in clinical diagnosis and decision-making. This wearable approach can in principle be adapted for the on-demand assessment of other trace-level and disease-relevant protein biomarkers.

Methods

Materials and reagents

Silver nitrate, iron(III) chloride and hydrogen tetrachloroaurate(III) hydrate were purchased from Alfa Aesar. Sodium thiosulfate pentahydrate, sodium bisulfite, 2-(N-morpholino)ethanesulfonic acid (MES) hydrate, MUA, MCH, EDC, N-hydroxysulfosuccinimide sodium salt (sulfo-NHS), bovine serum albumin (BSA), hydroquinone, hydrocortisone, human immunoglobulin G (IgG), TH acetate salt, FITC–albumin conjugate, 1H-pyrrole-1-propionic acid (PPA), 1-pyrenebutyric acid (PBA), Tween 20, chloroacetamide (CAA), 4-(2-hydroxyethyl)-1-piperazineethanesulfonic acid (HEPES), calcium chloride, 3 kDa Amicon Ultra-0.5 centrifugal filter unit and urea were purchased from Sigma Aldrich. Potassium ferricyanide(III) and potassium ferrocyanide(IV) were purchased from Acros Organics. Potassium chloride, 96-well Nunc MaxiSorp flat-bottom plates, Pierce Protein Concentrators PES, 100,000 molecular weight cut-off (MWCO), 0.5 ml, lyophilized human tumour necrosis factor α (TNFα), trypsin, and Pierce C18 spin columns were purchased from Thermo Fisher Scientific. Agarose, sulfuric acid, hydrochloric acid, sodium carbonate anhydrous, sodium bicarbonate, sodium chloride, sodium dihydrogen phosphate, potassium hydrogen phosphate, potassium chloride, hydrogen peroxide (30% (w/v)), dimethylformamide (DMF), liquid chromatography–mass spectrometry (LC–MS)-grade acetonitrile (ACN), HPLC-grade water, folic acid, trifluoroacetic acid (TFA) and 10× PBS were purchased from Fisher Scientific. Twenty nanometre carboxyl (carboxyl-PEG3000-SH) AuNPs were purchased from Cytodiagnostics. CRP cAbs and biotinylated dAbs were from the ELISA kit purchased from R&D systems (Human CRP DuoSet ELISA, DY1707). Recombinant human CRP protein standard was purchased from Abcam (ab167710). Medical adhesives were purchased from 3M and Adhesives Research. PI films (75 µm thick) were purchased from DuPont. PET films (50 µm thick) were purchased from McMaster-Carr. SureLight Peridinin-Chlorophyll Protein Complex (PerCP) was purchased from Assaybio. Lysyl endopeptidase was purchased from FUJIFILM Wako Chemicals.

Fabrication of the multiplexed microfluidic sensor patch

A PI film was raster-engraved at focus height (8% power, 15% speed and 1,000 points per inch (PPI)) to fabricate LEG-based iontophoresis electrodes; connection leads; and impedance, CRP working, counter and reference electrodes using a 50 W CO$_2$ laser cutter (Universal Laser System). The pH electrode and temperature sensor were engraved using vector mode with 1% and 3% power, respectively (15% speed and 1,000 PPI). The working electrode of the pH sensor was prepared by electrochemically cleaning the LEG electrode in 1 M HCl via cyclic voltammetry from −0.2 V to 1.2 V at 0.1 V s^{-1} for 10 cycles, followed by electrodeposition of polyaniline pH-sensing membrane via cyclic voltammetry from −0.2 V to 1.2 V at 0.1 V s^{-1} for 10 cycles. The shared Ag/AgCl reference electrode was fabricated by electrodeposition of Ag on the LEG electrode in a solution containing silver nitrate, sodium thiosulfate and sodium bisulfite (250 mM, 750 mM and 500 mM, respectively) using multi-current steps (30 s at −1 µA, 30 s at −5 µA, 30 s at −10 µA, 30 s at −50 µA, 30 s at −0.1 mA and 30 s at −0.2 mA), followed by drop-casting a 10 µl aliquot of 0.1 M iron(III) chloride for 1 min. AuNPs were electrodeposited on the LEG CRP working electrode via pulse deposition (two 0.5 s pulses at −0.2 V separated by a 0.5 s pulse at 0 V) for 40 cycles in the presence of 0.1 mM gold(III) chloride trihydrate and 10 mM sulfuric acid.

The iontophoresis hydrogels containing cholinergic agent carbachol (placed on the iontophoresis electrodes) were prepared by dissolving agarose (3% w/w) in deionized water using a microwave oven. After the agarose was fully dissolved, the mixture was cooled down to 165 °C and 1% carbachol for the anode (or 1% KCl for the cathode) was added to the above mixture and stirred to homogeneity. The cooled mixture was casted into cylindrical moulds or assembled microfluidic patch and solidified at room temperature. The hydrogels were stored at 4 °C until use.

To prepare the microfluidic module, an assembly of thin PET film (50 µm) sandwiched between double-sided medical adhesives (180 µm top layer and 260 µm bottom layer with a 50 µm PET backing) was attached to a substrate and cut through to make the channels and reagent reservoirs using the laser cutter at 2.7% power, 1.8% speed and 1,000 PPI vector mode. Next 4% power, 10% speed and 1,000 PPI vector mode was used to cut a circular outline through only the top layer of medical adhesive (180 µm). The circular top layer was peeled off to make the detection reservoir. A sweat accumulation layer was prepared by cutting through a 130 µm adhesive. The labelled dAb AuNPs were drop-casted and dried in the reagent reservoir and stored in dry state at 4 °C before assembly with the sensor patch.

LEG–AuNPs CRP working electrode functionalization

LEG–AuNPs working electrodes were immersed in 0.5 mM MUA and 1 mM MCH in proof 200 ethanol overnight for SAM formation. After rinsing with ethanol followed by deionized water and drying under airflow, electrodes were incubated with 10 µl of a mixture solution containing 0.4 M EDC and 0.1 M sulfo-NHS in 25 mM MES buffer, pH 5.0, for 35 min at room temperature in a humid chamber. Covalent attachment of CRP cAbs was carried out by drop-casting 10 µl of anti-CRP solution (250 µg ml^{-1} in PBS, pH 7.4) and incubated at room temperature for 2.5 h, followed by a 1 h blocking step with 1.0% BSA prepared in PBS. Electrodes were stored in 1% BSA in PBS until use.

CRP dAb conjugation

Twenty nanometre carboxylic acid-functionalized, PEGylated gold AuNPs were activated with EDC–sulfo-NHS mix solution (30 mg ml^{-1} and 36 mg ml^{-1}, respectively) in 10 mM MES buffer (pH 5.5) for 30 min. The conjugates were washed with 1× PBS containing 0.1% Tween 20 (PBST) and centrifuged at 6,500 relative centrifugal force (RCF) for 30 min. After supernatant removal, 50 µg ml^{-1} PS-R was added and allowed to crosslink for 1 h at room temperature. Following centrifugation at 3,500 RCF for 30 min and supernatant removal, 5 µg ml^{-1}

biotinylated anti-CRP dAb in 1% BSA prepared in 1× PBS (pH 7.4) was incubated for 1 h at room temperature. After another round of washing (centrifugation at 2,000 RCF), the carboxyl groups of PS-R and dAb on AuNP were activated with EDC–sulfo-NHS mix solution (30 mg ml⁻¹ and 36 mg ml⁻¹, respectively) in 10 mM MES buffer (pH 5.5) for 30 min. After the washing step using centrifugation at 1,500 RCF, 100 µM TH was incubated for 1 h. The final conjugate was washed with PBST, centrifuged at 1,250 RCF, reconstituted in 1% BSA and filtered through a 0.2 µm syringe filter to remove all aggregates.

For direct redox probe conjugation to antibodies, 100 µg ml⁻¹ dAb was buffer-exchanged by concentrating with a 100,000 MWCO protein concentrator and reconstituted in 10 mM MES buffer (pH 5.5). The carboxyl groups of the dAb were activated with EDC–sulfo-NHS mix solution (30 mg ml⁻¹ and 36 mg ml⁻¹, respectively) in 10 mM MES buffer (pH 5.5) for 30 min in column. Following buffer exchange with 1× PBS (pH 7.4), 100 µM TH was incubated for 1 h. The final conjugate was buffer-exchanged with PBS, reconstituted in 1% BSA and filtered through a 0.2 µm syringe filter to remove all aggregates.

Characterization of the biosensing method

The morphology and material properties of the LEG-based CRP sensing electrodes before and after surface modification were characterized by focused ion beam–scanning electron microscopy (FEI Nova 600 NanoLab), transmission electron microscopy (TecnaiTF-20), Raman spectroscopy, XPS (Kratos Ultra XPS) and UV–vis spectroscopy. Raman spectra of the electrodes were recorded using a 532.8 nm laser with an inVia Reflex (Renishaw). Dynamic light scattering data were collected using a Malvern Dynamic Light Scattering Zetasizer. UV–vis absorbance data were collected using a BioTek Synergy HTX multi-mode reader.

In vitro electrochemical characterizations were carried out on a CHI660e electrochemical workstation with a commercial Ag/AgCl electrode as the reference electrode.

Specifically, to characterize surface modification after each step electrochemically, DPV and open circuit potential–electrochemical impedance spectroscopy readings were obtained in 0.1 M KCl, containing 5.0 mM of $K_4Fe(CN)_6$–$K_3Fe(CN)_6$ (1:1) under the following conditions: potential range, −0.2 V to 0.6 V; pulse width, 0.2 s; incremental potential, 4 mV; amplitude, 50 mV; frequency range, 0.1–10⁶ Hz; amplitude, 5 mV.

Comparison of sensing performance with bare graphene-modified sensors was conducted following protocols published previously[43,61]. Briefly, the LEG electrodes were electrodeposited with poly(propionic acid) (PPA) via cyclic voltammetry or modified with PBA via π–π stacking by immersing the electrodes in 5 mM PBA prepared in DMF for 2 h. LEG was electrochemically oxidized in PBS (1×, pH 3) at +1.75 V for 45 s to produce graphene oxide. Next the LEG electrodes were activated with EDC–sulfo-NHS and incubated with cAbs (250 µg ml⁻¹ in PBS, pH 7.4) for 2.5 h. To compare the electrochemical performance, the cAb-modified electrodes were incubated in 0 ng ml⁻¹ or 10 ng ml⁻¹ CRP in 1% BSA for 15 min, followed by 15 min incubation in 1 µg ml⁻¹ horseradish peroxidase (HRP)-conjugated anti-CRP dAbs. Amperometric readings were recorded at 0 V in 50 mM sodium phosphate buffer (pH 6.0) containing 2.0 mM hydroquinone and 10 mM H_2O_2.

Electrochemical detection of CRP in buffer and biofluids was performed by mixing 4.5 µl aliquots of CRP standards (or raw biofluids to be analysed) with 0.5 µl dAb-loaded AuNPs (1:10 dilution prepared in 10% BSA in 1× PBS, pH 7.4) and drop-casting onto the working electrode, allowing CRP and dAb binding to take place for 15 min before rinsing with PBS. SWV was used to record the CRP signal in 1× PBS, pH 7.4. SWV conditions were as follows: potential range, 0 to −0.6 V; increment potential, 10 mV; amplitude, 50 mV; frequency, 25 Hz. The performance of the CRP sensors subjected to different incubation and detection conditions was evaluated from pH 6 to pH 10 and from 0.1× to 2× PBS. A selectivity test was conducted in the presence of a mixture of solutions of 1:100 dAb-loaded AuNPs (final concentration) and 5 ng ml⁻¹ cortisol, IgG, TNFα and CRP in the presence of 5 ng ml⁻¹ CRP.

The influence of mechanical deformation on the sensor performance was investigated by incubating the sensor patch in CRP standards for 15 min or McIlvaine buffers for pH sensors under mechanical deformation (with radii of bending curvature 2.5 cm and 3.5 cm). The temperature sensor readings were recorded by placing the patch in an oven under mechanical deformation.

Evaluation of the microfluidic module

The microfluidic module was evaluated with both numerical simulation and experimental flow tests.

Numerical simulation. Simulation of the CRP–antibody bonding reaction and mass transport process were conducted using the commercial software COMSOL Multiphysics through finite element analysis. Tetrahedral elements with refined meshes allowed modelling of the source diffusion in three-dimensional space with testified accuracy. The chemical reaction rate is described by law of mass action

$$r = k^f c_{CRP} \times c_{antibody} - k^r c_{complex}$$

where r, k^f, k^r, c_{CRP}, $c_{antibody}$ and $c_{complex}$ denote reaction rate, forward reaction coefficient, reverse reaction coefficient, concentration of CRP, concentration of antibody and concentration of CRP–antibody complex, respectively. The forward and reverse reaction coefficients are assumed to be 5.96×10^4 M⁻¹ s⁻¹ and 2.48×10^{-3} s⁻¹, respectively[62]. The concentration of CRP in sweat is assumed to be 1 ng ml⁻¹.

The fluid behaviour is described by the Navier–Stokes equation for incompressible flow

$$\rho \left(\frac{\partial v}{\partial t} + (v \cdot \nabla) v \right) = -\nabla p + \mu \nabla^2 v$$

$$\nabla \cdot v = 0$$

where ρ, v, t, p and μ denote liquid density, flow velocity, time, pressure and viscosity, respectively. The sweat flow rate is 1.5 µg ml⁻¹. The convection diffusion is described by

$$\frac{\partial c}{\partial t} + v \cdot \nabla c = D \nabla^2 c$$

where c and D denote the concentration and diffusion coefficient, respectively. The diffusion coefficient of CRP is 5×10^{-11} m² s⁻¹, and the diffusion coefficient of the antibody and CRP–antibody complex are set to be the same as AuNPs which is 1×10^{-12} m² s⁻¹.

Experimental flow tests. The flow tests to evaluate the microfluidic sensing system were done with a syringe pump (78-01001; Thermo Fisher Scientific). For the fluorescence flow test, a flow patch was pre-deposited with 0.5 µg PerCP and 200 µg BSA in the reagent reservoir and dried before full patch assembly, and 0.25 µg ml⁻¹ FITC–albumin in 1× PBS was injected into the patch placed on a blue-light transilluminator (Accuris SmartBlue Mini) at a flow rate of 1.5 µl min⁻¹. For the CRP sensor validation, 7 µl 2× PBS and 2 µl 10× dAb-loaded AuNP were deposited in the reagent reservoir and dried before full patch assembly, and artificial sweat (0.1× or 0.2× PBS) containing CRP (1 ng ml⁻¹ or 5 ng ml⁻¹) was injected into the patch at the specified flow rate. For on-body flow testing, an assembled flow patch pre-deposited with black dye in the reagent reservoir was attached onto a participant's arm after sweat induction by iontophoresis.

Electronic system design and integration

A two-layer FPCB was designed using Eagle CAD and Fusion 360. The FPCB outline was designed as a rounded rectangle (31.7 mm × 25.5 mm) the same size as the microfluidic sensor patch, such that the

patch can be inserted directly underneath the FPCB via a cut-out (10 mm × 3.8 mm). The electronic system is composed of a magnetic reed switch (MK24-B-3; Standex-Meder Electronics) and a voltage regulator (ADP162; Analog Devices) for power management; a boost converter (TPS61096; Texas Instruments), BJT array (BCV62C; Nexperia) and analogue switch (DG468; Vishay Intertechnology) for iontophoretic induction; an electrochemical front-end (AD5941; Analog Devices), an operational amplifier (LPV811; Texas Instruments) and a voltage divider for sensor array interface; and a BLE module (CYBLE-222014-01; Cypress Semiconductor) programmed via PSoC Creator 4.3 for system control and Bluetooth wireless communication. A BLE dongle (CY5677; Cypress Semiconductor) programmed via PSoC Creator 4.3 or custom mobile application programmed via Flutter was used to establish a BLE connection with the wearable device and to wirelessly acquire sensor data for calibration and voltammogram analysis. A rechargeable 3.8 V lithium button cell battery with capacity of 8 mAh was used to power the electronic system. To reduce the existing noise caused by motion artefacts, filtering and smoothing techniques were used. On the hardware side, the electrochemical AFE filters noise from the ADC via digital filters. On the software side, smoothing algorithms (moving average filter or median filter) are automatically applied in real time.

Participants and procedures

The performance of the wearable sensor was evaluated in human sweat and saliva samples from healthy participants and from participants who had recently recovered from COVID-19 infection, in compliance with the protocols that were approved by the institutional review board (IRB) (numbers 19-0892, 19-0894 and 21-1108) at the California Institute of Technology (Caltech). The participants were recruited from the Caltech campus and neighbouring communities through advertisement by posted notices, word of mouth and email distribution. All participants gave written, informed consent before participation in the study.

Participants for the evaluation of the sweat CRP in COPD monitoring were recruited at The Lundquist Institute/Harbor–University of California, Los Angeles (UCLA) Medical Center with the protocol approved by the IRB at the Lundquist Institute (number 32051-01). Men and women, current or former smokers with or without COPD were recruited. Inclusion criteria were as follows: aged 40–80 years, BMI between 18 kg m^{-2} and 40 kg m^{-2} and a >10 pack-year smoking history. Additional inclusion criteria for patients with COPD were as follows: forced expiratory volume in 1 s (FEV$_1$) to forced vital capacity of <0.7, FEV$_1$ <80%, modified Medical Research Council dyspnoea scale ≥2 and COPD assessment test >5. Exclusion criteria included: significant chronic disease, other than COPD; severe and/or uncontrolled medical conditions that could interfere with the study; malignancy within the previous 2 years; HIV infection; active tuberculosis; documented cardiovascular disease or resting ECG abnormality; use of systemic corticosteroids; COPD exacerbation within 3 months; and those requiring supplemental oxygen.

Adult patients with a diagnosis of HF were recruited from the UCLA Ahmanson Cardiomyopathy Clinic, and the protocol was approved by the UCLA IRB (number 19-000388). Exclusion criteria included pregnancy, severe skin allergy, current need for inpatient hospitalization, current use of beta-blocker medication therapy due to theoretical interaction with pilocarpine, active inotropic medication infusion, hypotension or hypertension, severe bradycardia or tachycardia or significant cardiac conduction disorder.

Participants for the evaluation of the sweat CRP in infection monitoring were recruited with a protocol approved by the IRB at Cedars-Sinai Medical Center (number STUDY00001099). Enroled patients were those admitted to the hospital at ≥18 years of age who had an active infection (such as pneumonia, urinary tract infection or cellulitis).

Sample collection for in vitro studies. An iontophoresis session was implemented using a Model 3700 Macroduct Sweat Collection System for sweat induction; the participants were asked to wear a Macroduct collector over a period of 60 min for sweat collection. Participants were asked to refrain from eating, drinking and chewing gum 30 min before saliva collection. After rinsing mouth with water, volunteers deposited saliva in 1.5 ml Eppendorf tubes, which were subsequently centrifuged at 10,000 rpm for 10 min and analysed. Fresh blood samples were collected at the same periods of time as saliva and/or sweat, either using a finger-prick approach or via venous blood draw. Once the standardized clotting procedure finished, serum was separated by centrifuging at 3,575 rpm for 15 min, and instantly stored at −80 °C.

Human sample analysis with ELISA. ELISA tests for CRP were performed in an accuSkan FC Filter-Based Microplate Photometer at a detection wavelength of 450 nm, according to the manufacturer's instructions. Briefly, a 96-well Nunc MaxiSorp flat-bottom plate was modified with anti-CRP antibodies in 50 mM carbonate buffer (pH 9.6) overnight at 4 °C. Standards or diluted biofluid samples prepared in 1% BSA were added to anti-CRP antibody-coated microtiter plate wells and incubated for 2 h at room temperature. After three washing steps with wash buffer (PBST, pH 7.4), biotinylated detector antibodies were added to each well and incubated for 2 h at room temperature. After three washing steps, streptavidin–HRP was added and incubated for 20 min a room temperature. Following three washing steps, 100 μl 3,3′,5,5′-tetramethylbenzidine (TMB) substrate was incubated for 15 min, and absorbance values were measured immediately after the addition of 50 μl of 1 M H$_2$SO$_4$ to each well.

Human sample analysis with LC–MS/MS. A 1 ml pooled sweat sample was concentrated using Amicon centrifugal filters with an MWCO of 3 kDa to 15 μl final volume at a concentration factor of 67×. The concentrated samples were buffer-exchanged in 8 M urea in 10 mM HEPES buffer (pH 7.4), reduced with 3.7 mM tris(2-carboxyethyl)phosphine (TCEP) for 20 min at 37 °C and alkylated with 10 mM CAA for 15 min at 37 °C. Proteins from each sample were digested at 37 °C lysyl endopeptidase at a 1:100 ratio for 2 h. The samples were then diluted with 50 mM HEPES buffer (pH 7.4) to a final concentration of 2 M urea and digested with trypsin at a 1:50 ratio at 37 °C for 14 h. Digested peptides were acidified with 20% TFA and desalted with C18 spin columns using 50% ACN as the activation solution, 0.5% TFA in 5% ACN as the equilibration solution and wash solution, 2% TFA in 20% ACN as the sample buffer and 0.2% formic acid (FA) in 70% ACN as the elution buffer. Desalted peptides were freeze-dried and stored at −20 °C until use. Lyophilized peptide was reconstituted in 10 μl 0.2% FA in 2% ACN. All incubation procedures were carried out with shaking at 750 rpm in the dark.

LC–MS/MS analysis was performed with a Vanquish Neo UHPLC System (Thermo Fisher Scientific) coupled to an Orbitrap Eclipse Tribrid mass spectrometer (Thermo Fisher Scientific). Peptides were separated on an Aurora UHPLC Column (25 cm × 75 μm, 1.6 μm C18, AUR2-25075C18A; Ion Opticks) with a flow rate of 0.35 μl min^{-1} for a total duration of 75 min and ionized at 1.6 kV in the positive ion mode. The gradient was composed of 6% solvent B (3.5 min), 6–25% B (41.5 min), 25–40% B (15 min), 40–98% B (1 min) and 98% B (14 min), where solvent A was 0.1% FA in water, and solvent B was 80% ACN and 0.1% FA. MS1 scans were acquired at the resolution of 120,000 from 350 to 1,800 m/z, AGC target 1 × 10^6 and maximum injection time 50 ms. The charge states and intensity threshold of precursor ions for triggering MS2 was set to 2–7 and 5 × 10^3, respectively. For targeted CRP analysis, the precursor ions from the inclusion list (Supplementary Table 1) were selected for MS2 spectrum acquisition in the ion trap using fast scan rate and quadrupole isolation mode (isolation window 1.2 m/z) with higher-energy collisional dissociation (30%) activation type. Dynamic exclusion was set to 30 s. The temperature of ion transfer tube was 300 °C and the S-lens radio frequency level was set to 30.

MS2 fragmentation spectra were searched with Proteome Discoverer SEQUEST (v.2.5; Thermo Scientific) against in silico tryptic-digested Uniprot Human database. The maximum missed cleavages was set to two. Dynamic modifications were set to oxidation on methionine (+15.995 Da), protein amino-terminal acetylation (+42.011 Da) and Met loss (−131.040 Da). Carbamidomethylation on cysteine residues (+57.021 Da) was set as a static modification. The maximum parental mass error was set to 10 ppm, and the MS2 mass tolerance was set to 0.6 Da. The false discovery threshold was set strictly to 0.01 using the Percolator node validated by q value. The relative abundance of parental peptides was calculated by integration of the area under the curve of the MS1 peaks using the Minora label-free quantification node.

On-body wearable evaluation. The participants' arm was cleaned with alcohol swabs and gauze before the wearable sensor patches were placed on the body. A 5 min iontophoresis was applied to the participant. During the on-body trial, the data from the sensor patches were wirelessly sent to the user interface via Bluetooth. The sensor system continuously acquired and transmitted impedance data from the ionic strength sensors. When the impedance data plateaued after an increase, the system would proceed with an SWV scan over the CRP sensor followed by the acquisition of the readings of pH and skin temperature sensors. After being real-time calibrated using simultaneously collected electrolyte and pH information, the acquired data were converted to the concentration levels based on the calibration curve.

Reporting summary

Further information on research design is available in the Nature Portfolio Reporting Summary linked to this article.

Data availability

The main data supporting the results in this study are available within the paper and its Supplementary Information. Source data for Figs. 3 and 5 are provided with this paper. All raw and analysed datasets generated during the study are available from the corresponding author on request.

References

1. The top 10 causes of death. *World Health Organization* https://www.who.int/news-room/fact-sheets/detail/the-top-10-causes-of-death (2020).
2. Mannino, D. M. et al. Economic burden of COPD in the presence of comorbidities. *Chest* **148**, 138–150 (2015).
3. Ferrucci, L. & Fabbri, E. Inflammageing: chronic inflammation in ageing, cardiovascular disease, and frailty. *Nat. Rev. Cardiol.* **15**, 505–522 (2018).
4. Ashley, N. T., Weil, Z. M. & Nelson, R. J. Inflammation: mechanisms, costs, and natural variation. *Annu. Rev. Ecol. Evol. Syst.* **43**, 385–406 (2012).
5. Schett, G. & Neurath, M. F. Resolution of chronic inflammatory disease: universal and tissue-specific concepts. *Nat. Commun.* **9**, 3261 (2018).
6. Furman, D. et al. Chronic inflammation in the etiology of disease across the life span. *Nat. Med.* **25**, 1822–1832 (2019).
7. Wylezinski, L. S., Gray, J. D., Polk, J. B., Harmata, A. J. & Spurlock, C. F. Illuminating an invisible epidemic: a systemic review of the clinical and economic benefits of early diagnosis and treatment in inflammatory disease and related syndromes. *J. Clin. Med.* **8**, 493 (2019).
8. Emerging Risk Factors Collaboration et al. C-reactive protein concentration and risk of coronary heart disease, stroke, and mortality: an individual participant meta-analysis. *Lancet* **375**, 132–140 (2010).
9. Ridker, P. M. A test in context: high-sensitivity C-reactive protein. *J. Am. Coll. Cardiol.* **67**, 712–723 (2016).
10. Proctor, M. J. et al. Systemic inflammation predicts all-cause mortality: a Glasgow inflammation outcome study. *PLoS ONE* **10**, e0116206 (2015).
11. Prins, B. P. et al. Investigating the causal relationship of C-reactive protein with 32 complex somatic and psychiatric outcomes: a large-scale cross-consortium Mendelian randomization study. *PLoS Med.* **13**, e1001976 (2016).
12. Balayan, S., Chauhan, N., Rosario, W. & Jain, U. Biosensor development for C-reactive protein detection: a review. *Appl. Surf. Sci. Adv.* **12**, 100343 (2022).
13. Young, B., Gleeson, M. & Cripps, A. W. C-reactive protein: a critical review. *Pathology* **23**, 118–124 (1991).
14. Lobo, S. M. Sequential C-reactive protein measurements in patients with serious infections: does it help? *Crit. Care* **16**, 130 (2012).
15. Guo, S., Mao, X. & Liang, M. The moderate predictive value of serial serum CRP and PCT levels for the prognosis of hospitalized community-acquired pneumonia. *Respir. Res.* **19**, 193 (2018).
16. Gao, W. et al. Fully integrated wearable sensor arrays for multiplexed in situ perspiration analysis. *Nature* **529**, 509–514 (2016).
17. Yang, Y. & Gao, W. Wearable and flexible electronics for continuous molecular monitoring. *Chem. Soc. Rev.* **48**, 1465–1491 (2019).
18. Ray, T. R. et al. Soft, skin-interfaced sweat stickers for cystic fibrosis diagnosis and management. *Sci. Transl. Med.* **13**, eabd8109 (2021).
19. Kim, J., Campbell, A. S., de Ávila, B. E.-F. & Wang, J. Wearable biosensors for healthcare monitoring. *Nat. Biotechnol.* **37**, 389–406 (2019).
20. Lee, H. et al. A graphene-based electrochemical device with thermoresponsive microneedles for diabetes monitoring and therapy. *Nat. Nanotechnol.* **11**, 566–572 (2016).
21. Koh, A. et al. A soft, wearable microfluidic device for the capture, storage, and colorimetric sensing of sweat. *Sci. Transl. Med.* **8**, 366ra165 (2016).
22. Ates, H. C. et al. On-site therapeutic drug monitoring. *Trends Biotechnol.* **38**, 1262–1277 (2020).
23. Bariya, M., Nyein, H. Y. Y. & Javey, A. Wearable sweat sensors. *Nat. Electron.* **1**, 160–171 (2018).
24. Parlak, O., Keene, S. T., Marais, A., Curto, V. F. & Salleo, A. Molecularly selective nanoporous membrane-based wearable organic electrochemical device for noninvasive cortisol sensing. *Sci. Adv.* **4**, eaar2904 (2018).
25. Tu, J., Torrente-Rodríguez, R. M., Wang, M. & Gao, W. The era of digital health: a review of portable and wearable affinity biosensors. *Adv. Funct. Mater.* **30**, 1906713 (2020).
26. Heikenfeld, J. et al. Accessing analytes in biofluids for peripheral biochemical monitoring. *Nat. Biotechnol.* **37**, 407–419 (2019).
27. Yang, Y. et al. A laser-engraved wearable sensor for sensitive detection of uric acid and tyrosine in sweat. *Nat. Biotechnol.* **38**, 217–224 (2020).
28. Yu, Y. et al. Biofuel-powered soft electronic skin with multiplexed and wireless sensing for human-machine interfaces. *Sci. Robot.* **5**, eaaz7946 (2020).
29. Sempionatto, J. R. et al. An epidermal patch for the simultaneous monitoring of haemodynamic and metabolic biomarkers. *Nat. Biomed. Eng.* **5**, 737–748 (2021).
30. Emaminejad, S. et al. Autonomous sweat extraction and analysis applied to cystic fibrosis and glucose monitoring using a fully integrated wearable platform. *Proc. Natl Acad. Sci. USA* **114**, 4625–4630 (2017).
31. Bandodkar, A. J., Jeang, W. J., Ghaffari, R. & Rogers, J. A. Wearable sensors for biochemical sweat analysis. *Annual Rev. Anal. Chem.* **12**, 1–22 (2019).

32. Xuan, X., Pérez-Ràfols, C., Chen, C., Cuartero, M. & Crespo, G. A. Lactate biosensing for reliable on-body sweat analysis. *ACS Sens.* **6**, 2763–2771 (2021).

33. Pirovano, P. et al. A wearable sensor for the detection of sodium and potassium in human sweat during exercise. *Talanta* **219**, 121145 (2020).

34. Garcia-Cordero, E. et al. Three-dimensional integrated ultra-low-volume passive microfluidics with ion-sensitive field-effect transistors for multiparameter wearable sweat analyzers. *ACS Nano* **12**, 12646–12656 (2018).

35. He, W. et al. Integrated textile sensor patch for real-time and multiplex sweat analysis. *Sci. Adv.* **5**, eaax0649 (2019).

36. Choi, D.-H., Kitchen, G. B., Jennings, M. T., Cutting, G. R. & Searson, P. C. Out-of-clinic measurement of sweat chloride using a wearable sensor during low-intensity exercise. *npj Digit. Med.* **3**, 49 (2020).

37. Zhong, B., Jiang, K., Wang, L. & Shen, G. Wearable sweat loss measuring devices: from the role of sweat loss to advanced mechanisms and designs. *Adv. Sci.* **9**, 2103257 (2022).

38. Lin, H. et al. A programmable epidermal microfluidic valving system for wearable biofluid management and contextual biomarker analysis. *Nat. Commun.* **11**, 4405 (2020).

39. Saldanha, D. J., Cai, A. & Dorval Courchesne, N.-M. The evolving role of proteins in wearable sweat biosensors. *ACS Biomater. Sci. Eng.* **9**, 2020–2047 (2021).

40. Mishra, R. K. et al. Continuous opioid monitoring along with nerve agents on a wearable microneedle sensor array. *J. Am. Chem. Soc.* **142**, 5991–5995 (2020).

41. Wang, B. et al. Wearable aptamer-field-effect transistor sensing system for noninvasive cortisol monitoring. *Sci. Adv.* **8**, eabk0967 (2022).

42. An, J. E. et al. Wearable cortisol aptasensor for simple and rapid real-time monitoring. *ACS Sens.* **7**, 99–108 (2022).

43. Torrente-Rodríguez, R. M. et al. Investigation of cortisol dynamics in human sweat using a graphene-based wireless mHealth system. *Matter* **2**, 921–937 (2020).

44. Jagannath, B. et al. Novel approach to track the lifecycle of inflammation from chemokine expression to inflammatory proteins in sweat using electrochemical biosensor. *Adv. Mater. Technol.* **7**, 2101356 (2022).

45. Gao, Y. et al. A flexible multiplexed immunosensor for point-of-care in situ wound monitoring. *Sci. Adv.* **7**, eabg9614 (2021).

46. Barkas, F., Liberopoulos, E., Kei, A. & Elisaf, M. Electrolyte and acid-base disorders in inflammatory bowel disease. *Ann. Gastroenterol.* **26**, 23–28 (2013).

47. Majewski, S. et al. Skin condition and its relationship to systemic inflammation in chronic obstructive pulmonary disease. *Int. J. Chron. Obstruct. Pulmon. Dis.* **12**, 2407–2415 (2017).

48. Yang, X. et al. Graphene uniformly decorated with gold nanodots: in situ synthesis, enhanced dispersibility and applications. *J. Mater. Chem.* **21**, 8096–8103 (2011).

49. Yu, Y. et al. All-printed soft human-machine interface for robotic physicochemical sensing. *Sci. Robot.* **7**, eabn0495 (2022).

50. Harshman, S. W. et al. The proteomic and metabolomic characterization of exercise-induced sweat for human performance monitoring: a pilot investigation. *PLoS ONE* **13**, e0203133 (2018).

51. Pinto-Plata, V. M. et al. C-reactive protein in patients with COPD, control smokers and non-smokers. *Thorax* **61**, 23–28 (2006).

52. Retamales, I. et al. Amplification of inflammation in emphysema and its association with latent adenoviral infection. *Am. J. Respir. Crit. Care Med.* **164**, 469–473 (2001).

53. Tonstad, S. & Cowan, J. L. C-reactive protein as a predictor of disease in smokers and former smokers: a review. *Int. J. Clin. Pract.* **63**, 1634–1641 (2009).

54. Simmonds, S. J., Cuijpers, I., Heymans, S. & Jones, E. A. V. Cellular and molecular differences between HFpEF and HFrEF: a step ahead in an improved pathological understanding. *Cells* **9**, 242 (2020).

55. Lakhani, I. et al. Diagnostic and prognostic value of serum C-reactive protein in heart failure with preserved ejection fraction: a systematic review and meta-analysis. *Heart Fail. Rev.* **26**, 1141–1150 (2021).

56. Butler, J. et al. Clinical and economic burden of chronic heart failure and reduced ejection fraction following a worsening heart failure event. *Adv. Ther.* **37**, 4015–4032 (2020).

57. Albar, Z. et al. Inflammatory markers and risk of heart failure with reduced to preserved ejection fraction. *Am. J. Cardiol.* **167**, 68–75 (2022).

58. Xin, Y., Zhou, J., Nesser, H. & Lubineau, G. Design strategies for strain-insensitive wearable healthcare sensors and perspective based on the Seebeck coefficient. *Adv. Electron. Mater.* **9**, 2200534 (2023).

59. Wang, M. et al. A wearable electrochemical biosensor for the monitoring of metabolites and nutrients. *Nat. Biomed. Eng.* **6**, 1225–1235 (2022).

60. Bandodkar, A. J. et al. Battery-free, skin-interfaced microfluidic/electronic systems for simultaneous electrochemical, colorimetric, and volumetric analysis of sweat. *Sci. Adv.* **5**, eaav3294 (2019).

61. Torrente-Rodríguez, R. M. et al. SARS-CoV-2 RapidPlex: a graphene-based multiplexed telemedicine platform for rapid and low-cost COVID-19 diagnosis and monitoring. *Matter* **3**, 1981–1998 (2020).

62. Zhuang, G., Katakura, Y., Omasa, T., Kishimoto, M. & Suga, K.-I. Measurement of association rate constant of antibody-antigen interaction in solution based on enzyme-linked immunosorbent assay. *J. Biosci. Bioeng.* **92**, 330–336 (2001).

Acknowledgements

Author contributions

W.G. and J.T. initiated the concept and designed the overall studies. W.G. supervised the work. J.T., J. Min and Y.S. led the experiments and collected the overall data. C.X., J.L., T.-Y.W., E.D. and T.-F.C. contributed to sensor characterization and validation. J. Moore, J.H., E.H., T.P., P.C., J.J.H. and H.B.R. contributed to the design of the human trials and to the system's evaluation in the participants. All authors contributed to data analysis and provided feedback on the paper.

Competing interests

The authors declare no competing interests.

Additional information

nature research

Corresponding author(s):   Wei Gao

Last updated by author(s):   May 18, 2023

Reporting Summary

Nature Research wishes to improve the reproducibility of the work that we publish. This form provides structure for consistency and transparency in reporting. For further information on Nature Research policies, see our Editorial Policies and the Editorial Policy Checklist.

Statistics

For all statistical analyses, confirm that the following items are present in the figure legend, table legend, main text, or Methods section.

n/a	Confirmed	
☐	☒	The exact sample size (n) for each experimental group/condition, given as a discrete number and unit of measurement
☐	☒	A statement on whether measurements were taken from distinct samples or whether the same sample was measured repeatedly
☒	☐	The statistical test(s) used AND whether they are one- or two-sided *Only common tests should be described solely by name; describe more complex techniques in the Methods section.*
☒	☐	A description of all covariates tested
☒	☐	A description of any assumptions or corrections, such as tests of normality and adjustment for multiple comparisons
☐	☒	A full description of the statistical parameters including central tendency (e.g. means) or other basic estimates (e.g. regression coefficient) AND variation (e.g. standard deviation) or associated estimates of uncertainty (e.g. confidence intervals)
☒	☐	For null hypothesis testing, the test statistic (e.g. F, t, r) with confidence intervals, effect sizes, degrees of freedom and P value noted *Give P values as exact values whenever suitable.*
☒	☐	For Bayesian analysis, information on the choice of priors and Markov chain Monte Carlo settings
☒	☐	For hierarchical and complex designs, identification of the appropriate level for tests and full reporting of outcomes
☐	☒	Estimates of effect sizes (e.g. Cohen's d, Pearson's r), indicating how they were calculated

Our web collection on statistics for biologists contains articles on many of the points above.

Software and code

Policy information about availability of computer code

Data collection	Mbed was used to programme the microcontroller. A CH Instrument was used for off-body sensor data collection. Comsol was used for simulations.
Data analysis	Origin 2018 was used to analyse all data, plot the data and calculate the statistical parameters. A custom mobile application programmed via Flutter was used to establish a BLE connection with the wearable device and to wirelessly acquire sensor data for calibration and voltammogram analysis.

For manuscripts utilizing custom algorithms or software that are central to the research but not yet described in published literature, software must be made available to editors and reviewers. We strongly encourage code deposition in a community repository (e.g. GitHub). See the Nature Research guidelines for submitting code & software for further information.

Data

Policy information about availability of data

All manuscripts must include a data availability statement. This statement should provide the following information, where applicable:

- Accession codes, unique identifiers, or web links for publicly available datasets
- A list of figures that have associated raw data
- A description of any restrictions on data availability

The main data supporting the results in this study are available within the paper and its Supplementary Information. Source data for Figs. 3 and 5 are provided with this paper. All raw and analysed datasets generated during the study are available from the corresponding author on request.

Field-specific reporting

Please select the one below that is the best fit for your research. If you are not sure, read the appropriate sections before making your selection.

☒ Life sciences ☐ Behavioural & social sciences ☐ Ecological, evolutionary & environmental sciences

For a reference copy of the document with all sections, see nature.com/documents/nr-reporting-summary-flat.pdf

Life sciences study design

All studies must disclose on these points even when the disclosure is negative.

Sample size	For the on-body evaluation of the wearable sensor, 10 participants were recruited (3 healthy, 3 with post-COVID infection, 3 as current smokers, 1 with COPD). For the COPD study, 3 current smokers with COPD, 8 current smokers without COPD, 4 former smokers with COPD and 5 former smokers without COPD, and 5 never-smokers without COPD were involved. Tor the heart-failure study, 7 healthy participants, 5 patients with heart failure with reduced ejection fraction, and 6 patients with heart failure with preserved ejection fraction were involved. For the current-infection study, 3 patients with active infection were sampled on two consecutive days. For the past-infection (post-COVID) study, 3 participants with mild symptoms and 3 participants with moderate symptoms were involved. Sample sizes were chosen on the basis of literature standards for proof-of-concept experiments.
Data exclusions	No data were excluded.
Replication	All attempts at replication were successful when following the device-fabrication process described in the paper.
Randomization	The device was fabricated with same process and was tested in all participants under the same conditions. Randomization was therefore not relevant to the study.
Blinding	Blinding was not relevant, because a blinding process wouldn't influence the sampling result.

Reporting for specific materials, systems and methods

We require information from authors about some types of materials, experimental systems and methods used in many studies. Here, indicate whether each material, system or method listed is relevant to your study. If you are not sure if a list item applies to your research, read the appropriate section before selecting a response.

Materials & experimental systems

n/a	Involved in the study
☐	☒ Antibodies
☒	☐ Eukaryotic cell lines
☒	☐ Palaeontology and archaeology
☒	☐ Animals and other organisms
☐	☒ Human research participants
☒	☐ Clinical data
☒	☐ Dual use research of concern

Methods

n/a	Involved in the study
☒	☐ ChIP-seq
☒	☐ Flow cytometry
☒	☐ MRI-based neuroimaging

Antibodies

Antibodies used	Anti-CRP capture antibodies and Anti-CRP detector antibodies.
Validation	Sandwich ELISA based on the supplier's information (https://www.rndsystems.com/products/human-c-reactive-protein-crp-duoset-elisa_dy1707#product-datasheets).

Human research participants

Policy information about studies involving human research participants

Population characteristics	Healthy participants and post-COVID participants with no active infection and skin allergies, male and female, current or former smokers and with or without COPD were recruited. The inclusion criteria were: ages 40–80 years; BMI, 18–40 kg m-2; >10 pack-year smoking history. Additional inclusion criteria for the COPD patients were: forced expiratory volume in 1 second / forced vital capacity (FEV1/FVC) <0.7; FEV1 < 80%; modified Medical Research Council (mMRC) dyspnea scale ≥2; COPD Assessment Test (CAT) >5. The exclusion criteria included: significant chronic disease, other than COPD; severe and/or uncontrolled medical conditions

that could interfere with the study; malignancy within the previous 2 years; HIV infection; active tuberculosis; documented cardiovascular disease or resting ECG abnormality; use of systemic corticosteroids; COPD exacerbation within 3 months; those requiring supplemental oxygen. For adult patients with a diagnosis of heart failure, exclusion criteria included pregnancy, severe skin allergy, current need for inpatient hospitalization, current use of beta-blocker medication therapy due to theoretical interaction with pilocarpine, active inotropic medication infusion, hypotension or hypertension, severe bradycardia or tachycardia, or significant cardiac conduction disorder, and patients admitted to the hospital ≥18 years of age that had an active infection (such as pneumonia, UTI or cellulitis).

Recruitment

The participants were recruited from the Caltech campus, The Lundquist Institute/Harbor-UCLA Medical Center, the University of California, Los Angeles (UCLA) Ahmanson Cardiomyopathy Clinic, Cedars-Sinai Medical Center and the neighbouring communities through advertisement by posted notices, word of mouth, and email distribution. There were no self-selection biases or other biases.

Ethics oversight

California Institute of Technology, the Lundquist Institute/Harbor-UCLA Medical Center, UCLA Ahmanson Cardiomyopathy Clinic, and Cedars-Sinai Medical Center.

Note that full information on the approval of the study protocol must also be provided in the manuscript.